AD

USAAVLABS TECHNICAL REPORT 70-70

STUDY OF THE MECHANISMS OF SAND AND DUST EROSION

By

I. Finnie

December 1970

EUSTIS DIRECTORATE
U. S. ARMY AIR MOBILITY RESEARCH AND DEVELOPMENT LABORATORY
FORT EUSTIS, VIRGINIA

CONTRACT DAAJ02-68-C-0056
SOLAR DIVISION OF INTERNATIONAL HARVESTER COMPANY
SAN DIEGO, CALIFORNIA

46

A

100

DISCLAIMERS

The findings in this report are not to be construed as an official Department of the Army position unless so designated by other authorized documents.

When Government drawings, specifications, or other data are used for any purpose other than in connection with a definitely related Government procurement operation, the United States Government thereby incurs no responsibility nor any obligation whatsoever; and the fact that the Government may have formulated, furnished, or in any way supplied the said drawings, specifications, or other data is not to be regarded by implication or otherwise as in any manner licensing the holder or any other person or corporation, or conveying any rights or permission, to manufacture, use, or sell any patented invention that may in any way be related thereto.

DISPOSITION INSTRUCTIONS

Destroy this report when no longer needed. Do not return it to the originator.

DEPARTMENT OF THE ARMY
EUSTIS DIRECTORATE
U.S. ARMY AIR MOBILITY RESEARCH AND DEVELOPMENT LABORATORY
FORT EUSTIS, VIRGINIA

The research described herein was conducted by Professor Iain Finnie at the University of California, Berkeley, as a subcontract to Contract DAAJ02-68-C-0056 with the Solar Division of International Harvester. The work was performed under the technical management of David B. Cale, Propulsion Division, Eustis Directorate, U.S. Army Air Mobility Research and Development Laboratory.

Appropriate technical personnel of this Directorate have reviewed this report and concur with the conclusions and recommendations contained herein.

The findings outlined herein will be given consideration in the planning of future efforts in the area of sand and dust erosion of gas turbine engines.

Task 1G162203D14413
Contract DAAJ02-68-C-0056
USAAVLABS Technical Report 70-70
December 1970

STUDY OF THE MECHANISMS OF SAND AND DUST EROSION

Final Report
Solar Number RDR 1625-7

By

I. Finnie
University of California
Berkeley, California

Prepared by

Solar Division of International Harvester Company
San Diego, California

for

EUSTIS DIRECTORATE
U. S. ARMY
AIR MOBILITY RESEARCH AND DEVELOPMENT LABORATORY
FORT EUSTIS, VIRGINIA

ABSTRACT

The fundamental mechanisms by which erosion occurs in brittle solids have been examined.

The erosion process in brittle solids is studied by considering the extent to which a single impacting particle produces fracture in the surface of a brittle solid. By drawing on recent work on the location of fracture in brittle solids, it is possible to predict the effect of such variables as eroding particle size and velocity, angle of impact, material properties, and residual stress. Also, in the case of glass it is possible to predict, approximately, the particle size at which a transition occurs from brittle to ductile behavior.

TABLE OF CONTENTS

LIST OF ILLUSTRATIONS

LIST OF ILLUSTRATIONS (Cont)

LIST OF SYMBOLS

A	surface area
$A(x_o)$	area bounded by principal stress trajectory passing through x_o
a	radius of contact area
a	as an exponent to describe effect of sphere size on volume removal
a'	as an exponent to describe effect of abrasive particle size on volume removal
a^*	radius of outermost ring crack
$a = \dot{\phi}_o r/U$	a dimensionless parameter to describe particle rotation
c	fraction of particles cutting ductile materials
c	normalizing factor in Figure 18
E	modulus of elasticity
F_o	function defined in text
$F(\sigma)$	cumulative distribution function of σ
G_{IC}	critical value of energy release rate
$G(a^*)$	cumulative distribution function of a^*
H_o	function defined in text
K	constant used to describe ratio of vertical to horizontal forces in particle for ductile cutting. Used as constant in expression for stress in analysis of brittle erosion.
K_{IC}	plane strain fracture toughness
M	total mass of abrasive particles

LIST OF SYMBOLS (Cont)

m	a parameter in the Weibull distribution
m	mass of an abrasive particle
P	force on particle
p	pressure between particle and surface. In analysis of ductile erosion is the horizontal component of this pressure.
R	radius of sphere or average radius of irregular particle
R^*	effective radius used in analysing erosion by angular particles
R'	radius of cutting edge of angular particles
r	radial coordinate
S	depth of primary ring crack
$S_2(x_o)$	function defined in text
U	particle velocity
V	volume
V_p	volume removed by a particle
x	coordinate location
x_f	location of outermost value of x_o
x_G	coordinate of particle center of gravity in ductile cutting
x_o	location of horseshoe crack on x axis
x_t	coordinate of particle tip in ductile cutting
x_1 x_o	coordinates used in analysing erosion of brittle solids by oblique impact

LIST OF SYMBOLS (Cont)

y, y_1, y_o, y_t, y_G	similar to corresponding values of x
z	coordinate location
α	angle of impingement
β	coordinate used in Figure 10
Δs	distance used in Figure 10
μ	friction coefficient
ν	Poisson's ratio
ρ	density
σ_a	radial stress at rim of contact area when sphere is pressed against a surface
$\bar{\sigma}_a$	mean value of σ_a
σ_o	parameter in Weibull distribution
σ_u	parameter in Weibull distribution
$\sigma_x, \sigma_y, \tau_{xy}$	stress components on the surface of a solid loaded by a sphere
χ	depth of identation when sphere is pressed against surface

INTRODUCTION

The erosion of a surface by a stream of solid particles has received considerable attention in the past decade. About ten years ago, the primary motivation for erosion studies was the severe erosive wear that occurred in the equipment used for the catalytic cracking of oil.[1] Subsequently other situations have arisen in which erosion has been a problem; for example, in rocket nozzles and most recently in the compressors of helicopter engines. The economic importance of erosion in these and other applications had led to many valuable experimental studies. However, a detailed understanding of any type of wear, such that predictions can be made, depends on a knowledge of the mechanism by which material is being removed. Unfortunately, in many erosion studies this aspect has been treated superficially, if at all.

Clearly, the mechanism of erosion will not be the same for different types of materials, and to illustrate this, Figure 1 shows typical data for ductile and brittle materials. A ductile metal can undergo extensive plastic deformation, so during erosion by rigid abrasive grains we might expect the removal of material by chip formation or ploughing as in metal cutting or grinding. By contrast, in a brittle solid only elastic deformation occurs prior to fracture, and material must be removed by the propagation of cracks ahead of and around the impacting particle. The concepts of ideally ductile and ideally brittle behavior are, of course, oversimplified, but they do describe to a close approximation the behavior of many real materials and allow analytical solutions to be developed. Certainly, the mechanisms by which brittle and ductile solids erode must be understood before it will be possible to make an analysis for intermediate behavior.

In this report we will first examine the mechanism by which brittle solids erode and will then turn to the question of ductile solids. We consider, initially, only the case of perpendicular impact ($\alpha = 90$ deg in Fig. 1) and later will extend the results to the more general case of oblique impact.

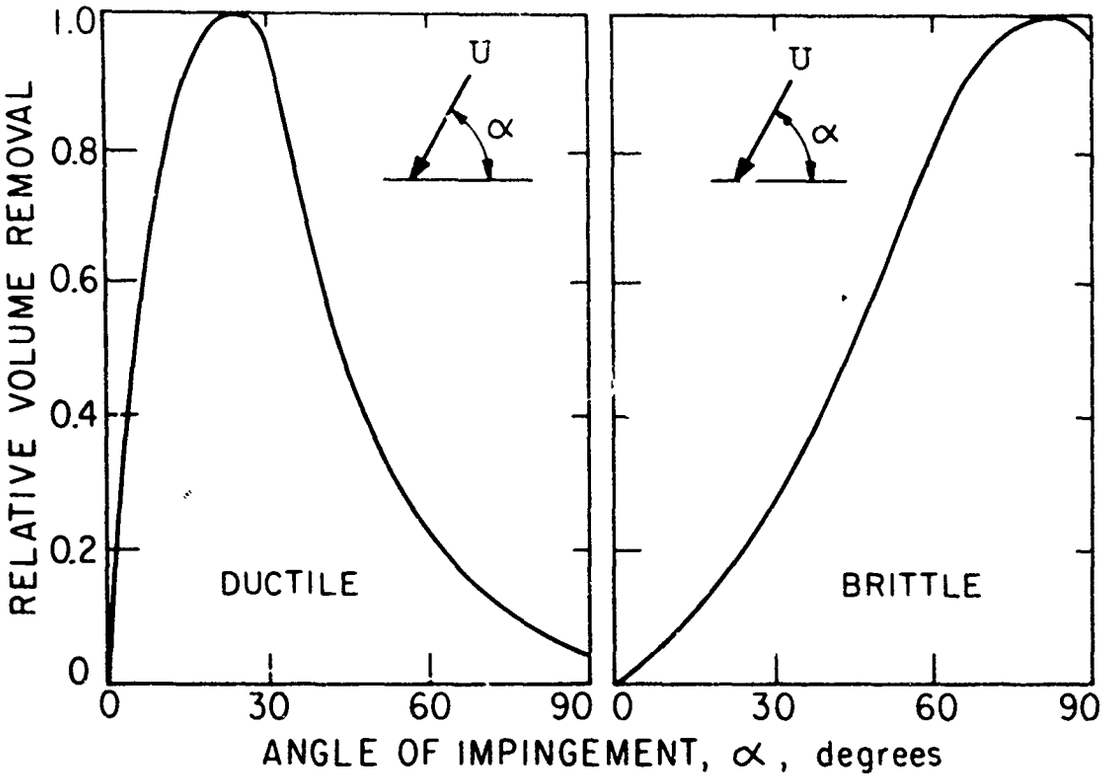

Figure 1. Volume Removed From a Surface by Erosion as a Function of the Angle of Impingement of the Eroding Particles (Shown Schematically For Ideally Ductile and Ideally Brittle Materials).

EROSION OF BRITTLE SOLIDS

In contemplating an analysis of brittle erosion, one might think first of an energy approach in which the volume removal is taken as proportional to the kinetic energy of the impacting particles or to the kinetic energy lost by the impacting particles during erosion. This type of approach is often followed in rock-drilling studies and enables crude predictions of volume removal to be made. However, the values reported for "energy required per unit volume crushed", i.e. the specific energy, vary greatly for a given type of rock, and it seems most unlikely that we could make detailed predictions about the role of particle size, particle velocity, impact angle, etc., on this basis. Studies of the crushing of brittle solids show that the essential energy requirement, that to produce fresh surface, is a very small and unpredictable fraction of the total energy expended in crushing[2]. So unless fragment size and surface area can be predicted in advance, it would appear to be most unrealistic to use a model based on energy to study erosion.

In the fields of rock mechanics and coal mining, analyses have been made of the chipping that occurs under an indenting tooth or wedge. The solutions apply only when the included angle of the wedge is small, so that chipping rather than crushing occurs, and do not appear to be applicable to the problem we are considering.

Since volume removal in brittle solids occurs by fracture, we decided to approach erosion by looking at the cracking that occurs when an idealized abrasive particle of spherical shape strikes the surface. This led us into a study of the fracture of brittle solids by spherical indenters. Some of this work will be summarized and applied to make erosion predictions.

We consider the case of a sphere pressed against a semi-infinite solid by a static force P or striking the plate with velocity U. The elastic solution due to Hertz and Huber is well known (e.g., it has been summarized by Timoshenko[3]). It shows that the surface stresses, prior to fracture, are compressive within the contact area and that outside, on the free surface, the radial stress is tensile while the circumferential stress is of equal magnitude but compressive. Below the surface, in the z-direction, the tensile stress decreases very rapidly. Figure 2 shows the variation of the radial tensile stress, on the free surface, with radius R. It is known [3] that the impact problem is pseudo static up to very high velocities; hence the maximum load P corresponding to a given impact velocity U may be shown to be

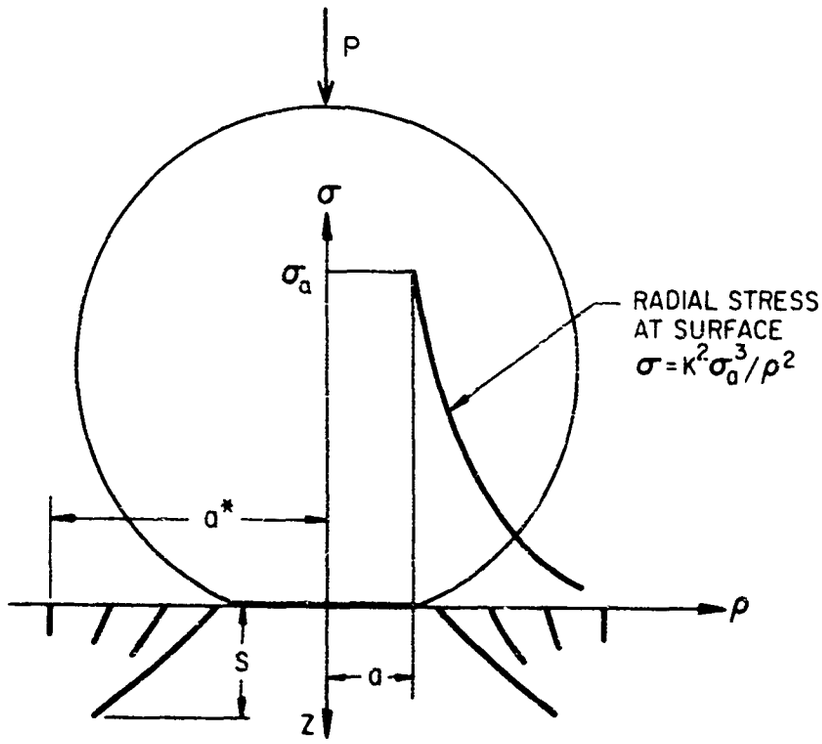

Figure 2. Coordinate System Used in Study of Ring Cracking.

$$P_{max} = \frac{\frac{4}{3}\left[\frac{5}{4}\pi\rho_1\right]^{\frac{3}{5}} U^{\frac{6}{5}} R^2}{\left[\frac{1-\nu_1^2}{E_1} + \frac{1-\nu_2^2}{E_2}\right]} \qquad (1)$$

where ρ_1 is the mass density of the sphere

ν_1 is the Poisson's ratio of the sphere

ν_2 is the Poisson's ratio of the surface

E_1 is the Young's modulus of the sphere

E_2 is the Young's modulus of the surface.

Fracture, when it first occurs, appears as a ring on the surface, usually well outside the contact area, and spreads out below the surface to form the frustum of a cone. If loading is continued, the initial crack spreads deeper into the solid

and additional concentric ring cracks form at successively greater radii.* Eventually, at a high enough load or velocity, extensive crushing occurs under the indenter. This behavior is illustrated in Figure 3, where we have used a relatively large spherical particle for experimental convenience. For smaller spheres, the velocities at which initial cracking and subsequent crushing occur will be much greater than the values shown in Figure 3 and also much greater than the velocities encountered in most applications involving erosion. For this reason, we base our analysis of erosion on the type of cracking shown in Figure 2.

In attempting to predict ring cracking, there is little value in the classical concept that a brittle solid fractures when the tensile stress reaches a certain magnitude. The load required to produce ring cracking in glass shows a great deal of scatter. In addition, there is a strong size effect such that if the indenter size is decreased from, say, 1 inch to 0.01 inch, there is a threefold increase in the value of σ_a, the stress at the rim of the contact area, computed from the mean fracture load. These observations are not new, about 30 years ago they led Weibull[4] to propound his statistical theory of brittle strength.

Basically, Weibull's idea was that the flaws are distributed at random in brittle solids. These flaws are, in general, too small to be detectable, and so one cannot relate flaw size to strength as in the familiar "Linear Elastic Fracture Mechanics" approach. Rather, one has to test a large number of specimens and determine the probability of failure for a given stress level and specimen size. As the size of the stressed region decreases, the probability of finding a severe flaw decreases and as a consequence the mean stress at failure increases. Strangely enough, although the ring crack led Weibull to his statistical treatment of brittle strength, he did not analyze this problem in any detail. Recently, the ring-cracking of glass has been studied in some detail[5], and it has been shown that the mean fracture load, the standard deviation of fracture load, and the mean location of the initial ring-crack for indenters of various radii could be predicted from bending test data. Here, to illustrate the procedures followed, and to obtain a result which we will use later, we compute the distribution of the stress σ_a at the rim of the contact area.

Following Weibull[4], we take the probability $F(\sigma)$ that a specimen of volume V fractures under a uniform tensile stress $\leq \sigma$ as

---

*We have observed this type of cracking during tests on glass and by sectioning aluminum oxide specimens after testing.

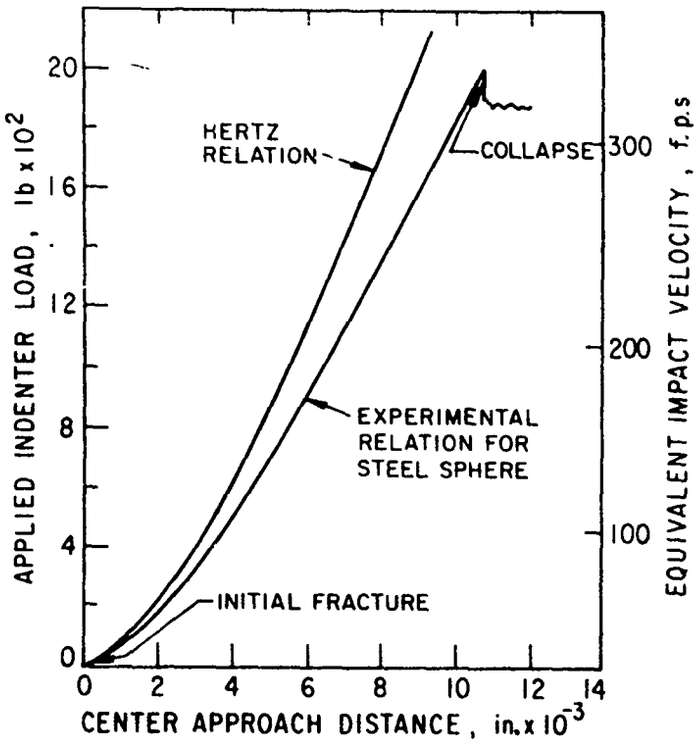

Figure 3. Variation of Approach of Center of 1/8 Inch Steel Ball to Undeformed Region of Glass Plate With Load. The Impact Velocities Corresponding to the Applied Loads Were Calculated From Equation 1.

$$F(\sigma) = 0 \qquad \sigma < \sigma_u$$

$$= 1 - e^{-V\left(\frac{\sigma - \sigma_u}{\sigma_o}\right)^m} \qquad \sigma > \sigma_u$$

where σ_u, σ_o, m -- the parameters of the probability distribution -- are assumed to be constants for a given material. If these constants are estimated, e.g., a number of tension tests on specimens of a given size, then this equation may be used to predict the probability of failure at a given level for other specimen sizes.

When the tensile stress, σ, is not uniform but varies over the volume, then the expression $(\sigma - \sigma_u/\sigma_o)^m$ is integrated over the volume stressed in tension.

$$F(\sigma) = 1 - e^{-\int_V \left(\frac{\sigma - \sigma_u}{\sigma_o}\right)^m dV} \qquad \sigma > \sigma_u$$

$$= 0 \qquad \sigma \leq \sigma_u$$

In this form the Weibull distribution may be used, for example, to make predictions about the distribution of bending strength values.

Glass is a brittle solid which is convenient for experimental work. However, unlike polycrystalline ceramics in which the strength-imparing flaws are distributed throughout the volume, glass inevitably fails due to surface flaws. Thus, if the preceding equations are applied to glass, V must be taken as the surface area stressed in tension.

For ball indentation on glass, the Weibull distribution takes the form

$$F(\sigma_a) = 1 - e^{\int_A \left(\frac{K^2 \sigma_a{}^3/\rho^2 - \sigma_u}{\sigma_o}\right)^m 2\pi\rho d\rho} \qquad \sigma_a > \sigma_u$$

$$= 0 \qquad \sigma_a \leq \sigma_u$$

when we have expressed the radial tensile stress, σ, in terms of the maximum tensile stress σ_a and integrated over the surface area where tensile stress exists. From this distribution we may calculate, for example, the average value of σ_a at fracture.

$$\text{Average } \sigma_a = \bar{\sigma}_a = \int \sigma_a dF(\sigma_a)$$

After obtaining the parameters σ_u, σ_o, m, in this case from bending tests[5], the computation may be carried out and gives the results shown in Figure 4. The agreement with experiment is reasonable over a wide range of indenter sizes.

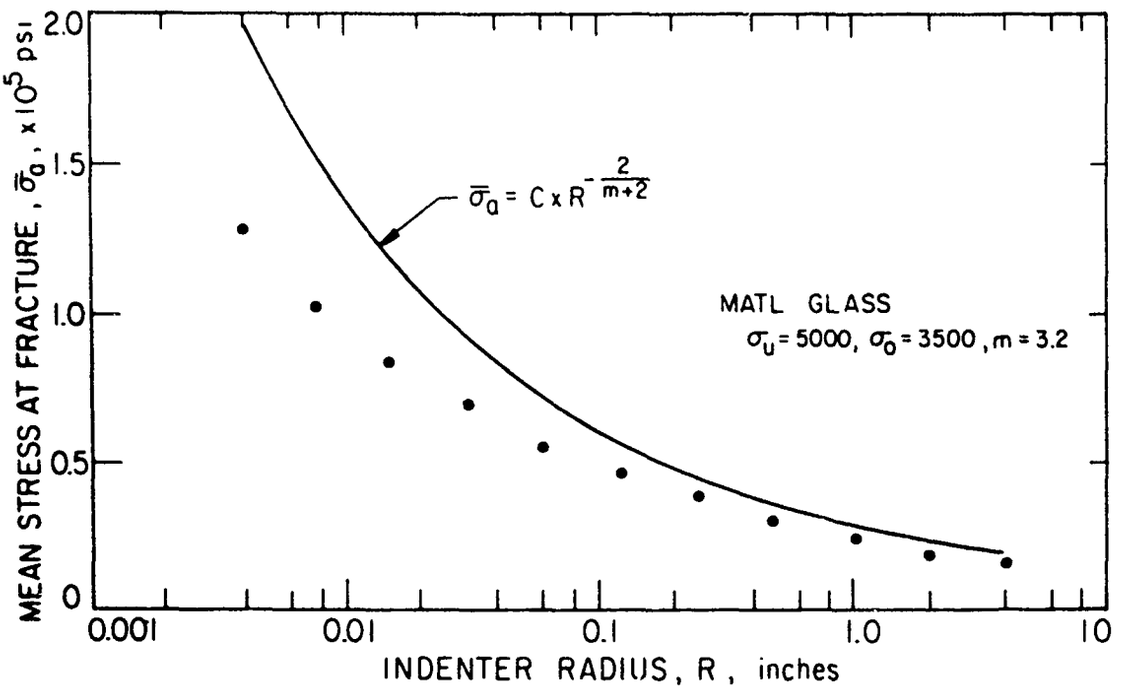

Figure 4. Predicted and Experimentally Determined Values of σ_a as a Function of Indenter Size.

It is also possible to use a two-parameter Weibull distribution for the calculations by taking $\sigma_u = 0$*. This may lead to less accurate predictions but often allows closed-form solutions to be obtained. In the case of ball indentation on glass plates, the two-parameter Weibull distribution leads to the prediction

$$\bar{\sigma}_a = (\text{constant}) R^{-\frac{2}{m+2}} \tag{2}$$

Another quantity that is of interest in erosion analysis is the location of the outermost ring crack. The subject of fracture location has seldom been considered in fracture studies and has never formed part of the Weibull theory. However, by extending the Weibull approach and looking at the probability of failure of differential elements which compose the solid, we may derive the distribution of fracture location.

---

* The values of the parameters σ_0 and m are now, in general, different from those found for the three-parameter distribution.

For a given load in ball indentation, if we divide the region under tension into concentric differential annuli, we can formulate the distribution of the outermost ring crack location as:

$$\text{Prob.}\begin{bmatrix}\text{outermost ring crack}\\ \text{occurs at a radius } a^*\end{bmatrix} = \text{Prob.}\begin{bmatrix}\text{the annulus at location}\\ a^* \text{ fails}\end{bmatrix} \times \text{Prob.}\begin{bmatrix}\text{all annuli exterior}\\ \text{to this annulus survive}\end{bmatrix}$$

This formulation has been carried out in detail[6], and it is shown that aside from elastic constants of the materials, the distribution of the outermost ring crack location G(a*) is also a function of Weibull parameters m, σ_u, σ_o, the indenter radius R, and the stress level in the solid, σ_a. That is,

$$G(a^*) = f(\sigma_u, \sigma_o, m, \sigma_a, R) \tag{3}$$

Figure 5 shows the calculated result for G(a*) when a glass plate (m = 3.2, σ_u = 5,000, σ_o = 3,500) is loaded by a 3/32-inch-radius indenter up to a load of 154 pounds. The agreement between prediction and experiment is quite satisfactory, particularly in view of the complex nature of the multiple type of fracture being considered.

SPHERICAL PARTICLES IMPACTING AT $\alpha = 90°$

We are now in a position to analyze the erosion of brittle solids and consider first the case of perpendicular impact ($\alpha = 90°$) by spherical particles. In all the work, we assume that the eroding particle is elastic and does not fracture during impact. By examining fracture patterns such as those shown in Figure 2, and noting that the radius a* is considerably larger than a, it seems reasonable to make the volume damaged by a single eroding particle V_p as

$$V_p \propto \overline{(a^{*2})}\, S$$

where $\overline{a^{*2}} = \int a^{*2}\, d\, G(a^*)$ is the average value of a*, and S is the depth of the primary ring crack as shown in Figure 2. Examination of ring cracks in glass indicates that the depth of the primary ring crack is proportional to the depth X to which the sphere indents the surface. From Figure 3 we see that the Hertz

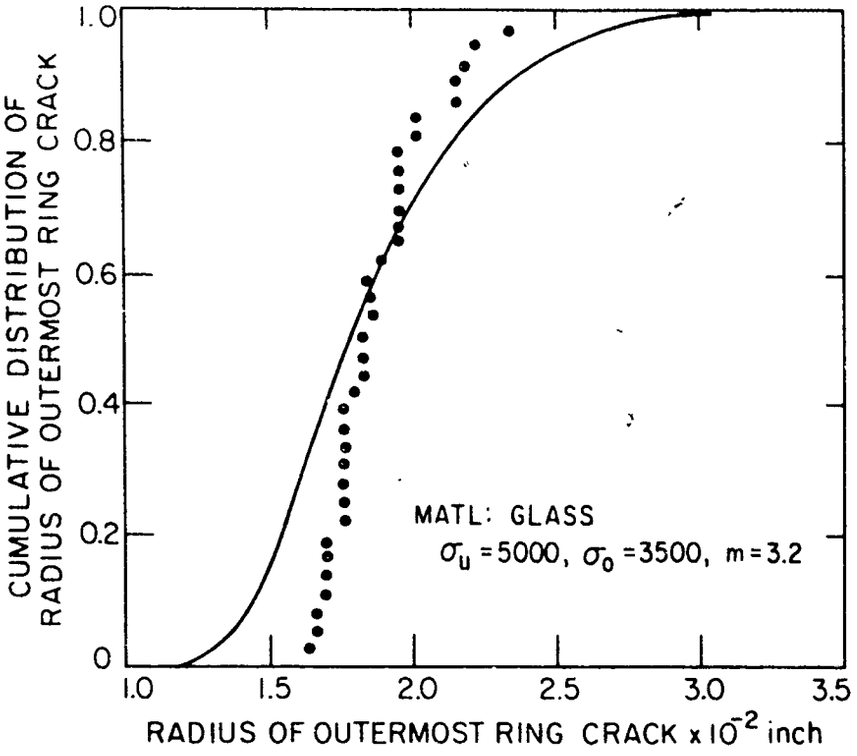

Figure 5. Predicted and Experimental Values for the Cumulative Distribution of the Outer Ring Crack When a Glass Plate is Loaded by a 3/32 Inch Indenter Under 154 Pounds.

equations provide a reasonable estimate of the load-deflection relation even after cracking occurs. Presumably this is due to the fact that the stresses are primarily compressive, and so even cracked material will transmit load.

Thus from the Hertz equations, we find

$$S \propto \chi \propto p^{2/3} R^{-1/3} \propto RU^{4/5}$$

so $V_p \propto RU^{4/5} \overline{a^{*2}}$. Since a* is a function of m, σ_u, σ_o, R and σ_a, where σ_a in turn depends on U, we now have an expression for the volume damaged by each particle which is a function only of R, U and the Weibull parameters (σ_o, σ_u, m). We examine this prediction, which requires numerical computation to evaluate the integral, by varying the Weibull parameter σ_u, holding the other four quantities (σ_o, m, R, U) constant. Effectively σ_u, the stress at or below which fracture does not occur, may be changed by inducing biaxial compressive stress in the surface. This was done by shrink-fitting steel rings onto glass disks. The predicted and observed values for relative volume removal are shown in Figure 6 and agree very well. As another test of our formulation, we took

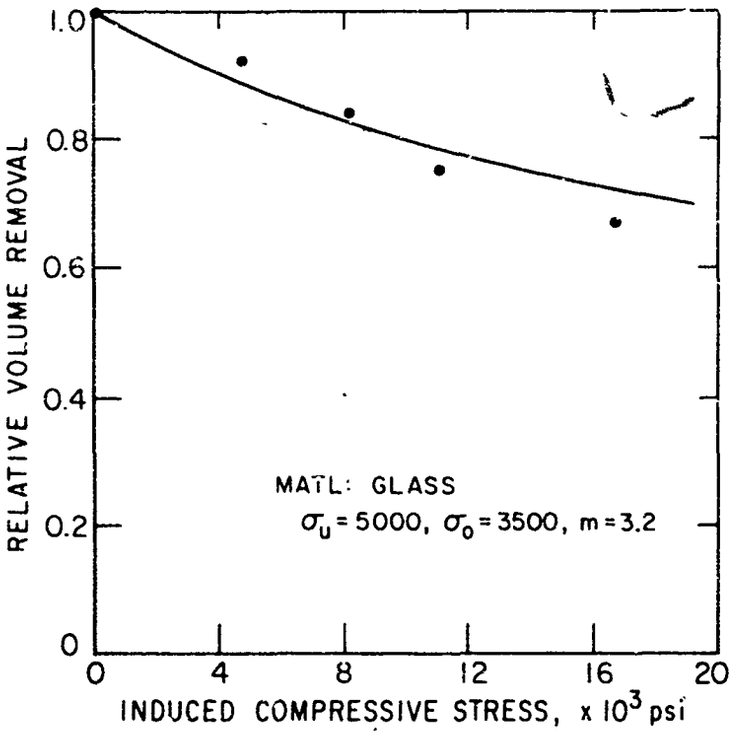

Figure 6. Influence of Biaxial Compressive Stress on Erosion of Glass at $\alpha = 90°$ by 0.0111 Inch Diameter Steel Shot at a Velocity of 270 ft/sec.

erosion data reported by Sheldon and Finnie[7] for three brittle solids which were eroded by spherical steel shot of various sizes at different velocities. The tester used in all our erosion studies is described in the Appendix. The observed volume removal per particle is plotted against $RU^{4/5}$ $(\overline{a^{*2}})$ in Figures 7, 8, and 9 for glass, magnesia and graphite respectively. For magnesia and graphite, $(\overline{a^{*2}})$ was computed by integrating over the volume stressed in tension rather than using area stressed in tension as in the case of glass. If the volume removed per particle is linearly proportional to the predicted volume damaged per particle, we expect the data points to fall on a straight line of slope unity. For magnesia and graphite this relation is indeed observed, while for glass the points fall on a straight line of slope 1.3. We speculate that the discrepancy in the case of glass is primarily due to the fact that the strength of glass in dynamic tests (erosion) is higher than in static tests (ring-cracking experiments). Possibly the use of the Weibull parameters obtained from dynamic tests would improve the prediction for glass.

SPHERICAL PARTICLES STRIKING AT OBLIQUE ANGLES

The extension of the preceding formulations to the case of oblique impact presents considerably difficulty. In this case the stress distribution around the indenter is

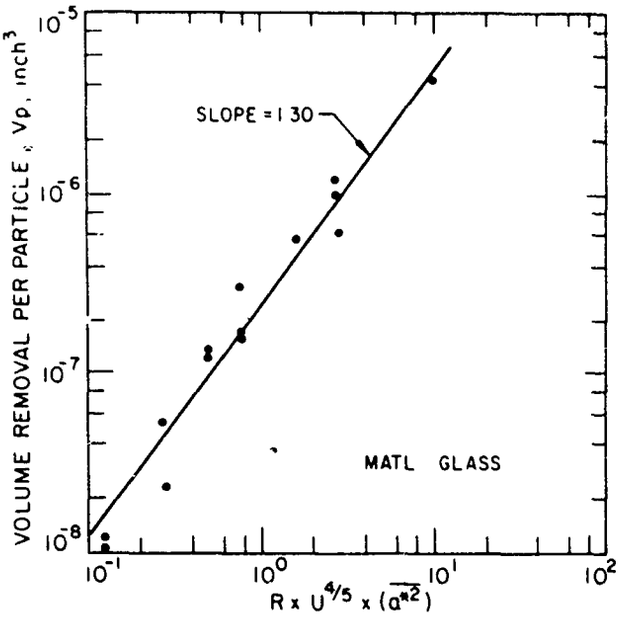

Figure 7. Experimentally Observed Values of Volume Removed Per Particle (for a Wide Range of Velocities and Particle Size) as a Function of the Predicted Damage Volume.

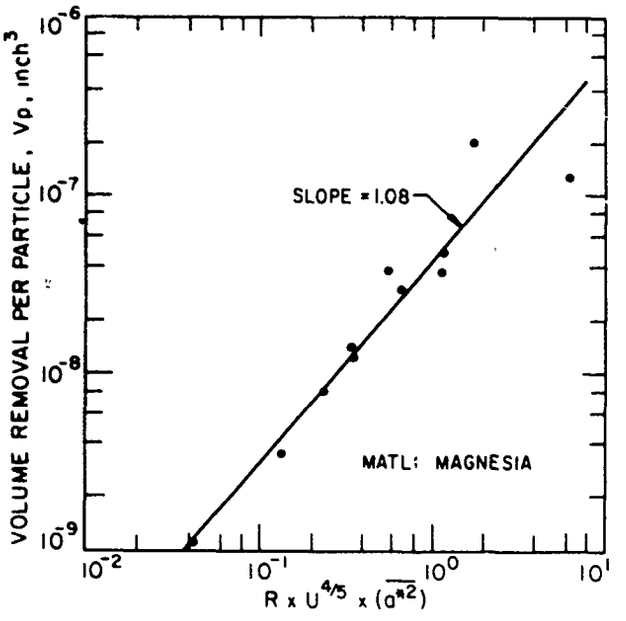

Figure 8. Experimentally Observed Values of Volume Removed Per Particle (for a Wide Range of Velocities and Particle Size) as a Function of the Predicted Damage Volume.

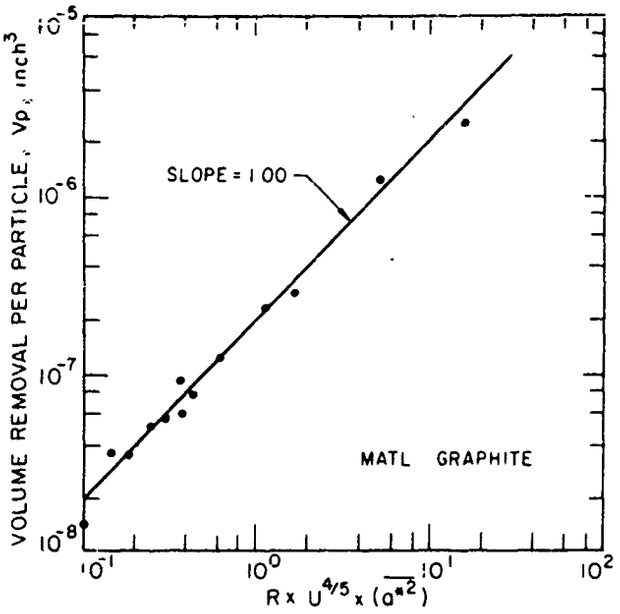

Figure 9. Experimentally Observed Values of Volume Removed Per Particle (for a Wide Range of Velocities and Particle Size) as a Function of the Predicted Damage Volume.

no longer axisymmetric because of the unidirectional frictional force. Thus, the ring cracks are distorted, and at relatively low values of horizontal force they become "horseshoe" shaped (open in the direction of sliding).

The stress distribution in the case of oblique elastic impact can be obtained by a superposition of the Hertzian stresses due to the normal component of the indenting force on the stresses due to the horizontal component. Using Cartesian coordinates (with xy lying in the surface and z pointing into the eroded material), and assuming a hemispherical distribution of frictional force in the contact area, such that the total traction is equal to the applied frictional force, Hamilton and Goodman[8] found for the contribution of the horizontal component alone when sliding takes place in the positive x direction:

$$\sigma_x = -\left(\frac{3\mu P}{2\pi a^3}\right)(xr^{-4})\left[2(r^2 + \nu_p y^2)F_o + \nu_p(3 - 4x^2 r^{-2})H_o\right] \quad (4)$$

$$\sigma_y = -\left(\frac{3\mu P}{2\pi a^3}\right)(\nu_p x r^{-4})\left[2x^2 F_o + (1 - 4y^2 r^{-2})H_o\right] \quad (5)$$

$$\tau_{xy} = -\left(\frac{3\mu P}{2\pi a^3}\right)(yr^{-4})\left[(r^2 - 2\nu_p x^2)F_o + \nu_p(1 - 4x^2 r^{-2})H_o\right] \quad (6)$$

for $r > a$ and $z = 0$, where ν_p is Poisson's ratio for the surface and

$$F_o = -\frac{1}{2} a(r^2 - a^2)^{1/2} + \frac{1}{2} r^2 \arctan \left[a(r^2 - a^2)^{1/2}\right] \quad (7)$$

$$H_o = \frac{1}{2} a(r^2 - a^2)^{3/2} - \frac{1}{4} r^4 \arctan \left[a(r^2 - a^2)^{-1/2}\right] - \frac{1}{4} ar^2(r^2 - a^2)^{1/2} \quad (8)$$

The stresses given by these equations may be combined with the Hertzian stresses

$$\sigma_x = \left(\frac{3P}{2\pi a^3}\right)\left[\frac{1}{3} a^3 (1 - 2\nu_p)\ (2x^2 r^{-4} - r^{-2})\right] \quad (9)$$

$$\sigma_y = \left(\frac{3P}{2\pi a^3}\right)\left[\frac{1}{3} a^3 (1 - 2\nu_p)\ (2y^2 r^{-4} - r^{-2})\right] \quad (10)$$

$$\tau_{xy} = \left(\frac{3P}{2\pi a^3}\right)\left[\frac{2}{3} a^3 (1 - 2\nu_p)\ x\ y\ r^{-4}\right] \quad (11)$$

for $r > a$, $z = 0$. Thus, the stress distribution on the surface is completely known once the load P, the coefficient of friction μ, and the contact radius a are defined. Stresses for $r < a$ and $z < 0$ are largely compressive and are not pertinent in the present study because fracture is assumed to originate from a region in tension.

Since fracture propagation follows a principal stress trajectory[9], it is assumed that for oblique impact, the volume removed is given by

$$V_p = (\text{constant}) \cdot \chi_m \cdot \text{Mean value of } A(x_o)$$

where χ_m is the maximum depth of indentation produced by the vertical component U sin α, and $A(x_o)$ is the area bounded by the outermost principal stress trajectory (PST) on the $z=0$ plane. Note that for zero coefficient of friction between the contacting surfaces, the stress distribution is Hertzian, and the prediction of volume removal is identical with the formulation for normal impact. The distribution of the outermost PST can be derived in a manner similar to that for the outermost ring fracture; namely, it is stipulated that the material outside the PST in question survives, and the material within fractures in at least one place. Numerically, however, the distribution of the outermost PST is much more difficult to evaluate.

Let a PST be described by its intercept on the negative x-axis, say, x_o, as shown in Figure 10. Thus, in a region with multiple cracks, the outermost x_o, denoted

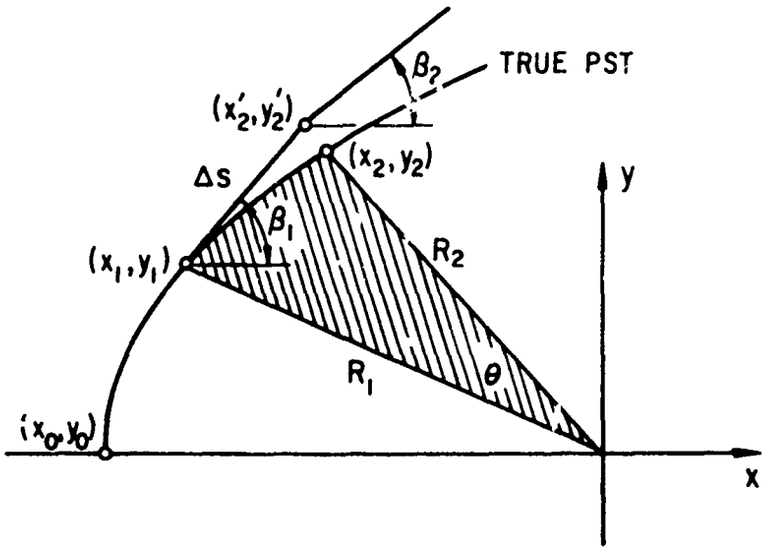

Figure 10. Numerical Method Used to Obtain Principal Stress Trajectory.

by x_f, will be a random variable whose distribution is related to the properties of the two bodies in contact, and the amount of indenting force. Now,

$$\text{Prob.}\,(X_f \le x_f) = \text{Prob. (the material outside the PST defined by } x_f \text{ survives the given load)} \times \text{Prob. (the material within fails)}$$

or

$$\text{Prob.}\left[X_f \le x_f\right] = e^{-\int_{\text{all } A > \text{PST}(x_f)} \left(\frac{\sigma_1 - \sigma_u}{\sigma_o}\right)^m dA} \cdot \left[1 - e^{-\int_{\text{all } A > \text{PST}(x_f)} \left(\frac{\sigma_1 - \sigma_u}{\sigma_o}\right)^m dA}\right]$$

$$= e^{-\int_{\text{all } A > \text{PST}(x_f)} \left(\frac{\sigma_1 - \sigma_u}{\sigma}\right)^m dA} - e^{-\int_{\text{all } A^o} \left(\frac{\sigma_1 - \sigma_u}{\sigma}\right)^m dA} \qquad (12)$$

for which the probability density function is

$$f_{x_f}(x_f) = e^{-\int_{\text{all } A > \text{PST}(x_f)} \left(\frac{\sigma_1 - \sigma_u}{\sigma_o}\right)^m dA} \times \frac{\delta}{\delta x_f} \int_{\text{all } A > \text{PST}(x_f)} \left(\frac{\sigma_1 - \sigma_u}{\sigma_o}\right)^m dA \qquad (13)$$

Obviously, numerical methods are necessary to evaluate this equation, which mainly involves the integral

$$\int_{\text{all } A > \text{PST}(x_f)} \left(\frac{\sigma_1 - \sigma_u}{\sigma_o}\right)^m dA = \int_y \int_x \left(\frac{\sigma_1 - \sigma_u}{\sigma_o}\right)^m dx\, dy \qquad (14)$$

in the plane $z = 0$ and the region outside the PST prescribed by x_f for which $\sigma_1 > \sigma_u$. This integral involves meticulous calculation and is a major task even with a high-speed computer. First, for $\mu > 0$, the stress distribution is highly complex. Great difficulty also arises in calculating the PST, for which there is no closed-form solution; then there is the evaluation of the integral itself by numerical methods. Nevertheless, a program was prepared to perform the following sequence of calculation:

THE PRINCIPAL STRESS TRAJECTORY

Referring to Figure 10, starting with $x_o = 0$ and $y_o = 0$, the direction of the principal stress is calculated using the equations for the stresses. A neighboring point with coordinates (x_1', y_1') is then defined by

$$x_1' = x_o + \Delta s \cos \beta_1 \qquad (15)$$

$$y_1' = y_o + \Delta s \sin \beta_1 \qquad (16)$$

where Δs is an arbitrary increment. At (x_1', y_1'), the direction of the principal stress, β_2, is again calculated, and a point supposedly on or near the PST is defined by

$$x_1' = x_1' + \Delta s \sin(\beta_1 - \beta_2) \sin \beta_2 \qquad (17)$$

$$y_1 = y_1' + \Delta s \sin(\beta_1 - \beta_2) \cos \beta_2 \qquad (18)$$

This procedure is then repeated to obtain another point (x_2, y_2), and so on. The points (x_0, y_0), (x_1, y_1), (x_2, y_2) . . . are then points on or near the PST which passes through (x_0, y_0). It is obvious that without Equations (17) and (18), the coordinates for the PST, which would have been calculated only by Equations (15) and (16), will be subject to cumulative errors. With Equations (17) and (18) it was possible to have virtually all the calculated points fall on the PST.

The area bounded by the PST, $A(x_0)$, is easily found once the coordinates of the points in the PST are known. In fact, $A(x_0)$ is found by summing the incremental areas A_i, shown shaded in Figure 10, which were calculated at the same time the coordinates (x_i, y_i) were being found. Thus, referring to Figure 10,

$$\Delta A_i = \left(\frac{R_1 + R_2}{2}\right)^2 \cdot \frac{\theta}{2} \tag{19}$$

where θ is in radians, and

$$A(x_o) = \sum \Delta A_i \tag{20}$$

The integral $\int_{\text{all } A > \text{PST}(x_o)} \left(\frac{\sigma_1 - \sigma_u}{\sigma_o}\right)^m dA$ is approximated by the sum

$$S_2(x_o) = \sum_{\text{all } x > x_o} \left[\sum_{\substack{\text{along} \\ \text{PST}(x_o)}} \left(\frac{\sigma_1 - \sigma_u}{\sigma_o}\right)^m \cdot \Delta s \right] \Delta x \tag{21}$$

The summand $(\sigma_1 - \sigma_u/\sigma_o)^m$. Δs in the inner sum is also calculated at the same time that the coordinates are found. The implication of this equation is that in the elemental area $\Delta s \cdot \Delta x$, the principal stress σ_1 is constant. Equation (21) accounts for only the shaded part of the total risk of rupture shown in Figure 11 and, as a result, will underestimate the integral by an amount which depends upon how the PSTs "diverge". At any rate, the errors in the preceding equation, as in Equations (15), (16), (17), and (18), can be minimized by making Δs and Δx as small as practical. It was found that for $\Delta s = 0.05x$ and $\Delta x = 0.01a$, the errors are insignificant in the sense that by making Δs or Δx smaller, there is very little change in the predicted erosion rate.

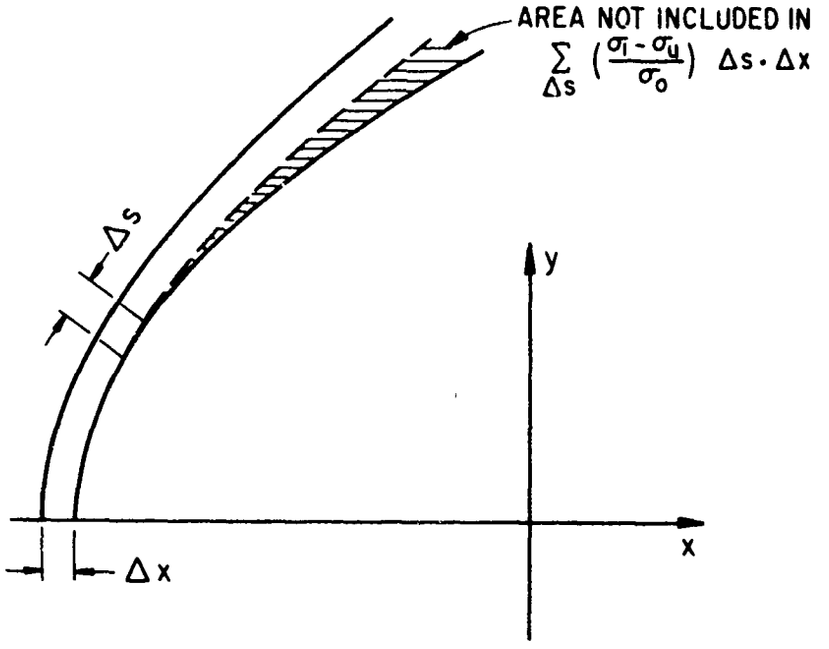

Figure 11. Error in the Numerical Method Used to Calculate Erosion Rate Under Oblique Impact Conditions.

Finally, with $A(x_o)$ and $S_2(x_o)$ stored in the memory of the computer for all $a \leq x_o \leq x_{ou}$ at an interval of $\Delta x = 0.01a$, where x_{ou} is the value of x_o beyond which $\sigma_1 < \sigma_u$, the average volume removal per particle is calculated by taking the product of the depth of indentation and the average value of $A(x_o)$. That is,

$$V_p = \text{const}\, \chi_m \int_{x_o = a}^{x_{ou}} A(x_o)\, f_{x_f}(x_o)\, dx_o \qquad (22)$$

where $f_{x_f}(x_o)$ may be found once the value of $S_2(x_o)$ is known. It is to be noted that in the evaluation, the equation for $S_2(x_o)$, a surface distribution of flaws, is assumed -- that flaws exist only on the surface, or at least that those underneath are insignificant compared to those on the surface insofar as fracture initiation is concerned. This assumption is probably justified in the case of glass, where from previous experience failure is known to initiate invariably from a surface flaw. In other brittle materials such as alumina, magnesia and graphite, the location of fracture is not clear, and hence there is some reservation regarding this assumption. In any case, the principal stress decays rapidly with the distance from the surface and becomes compressive at a distance of about 0.05a. Thus, treating the problem in this manner is probably not too far from the actual condition. The only unknown parameter in the analysis is the coefficient of friction between the sphere and the surface, for this determines the horizontal

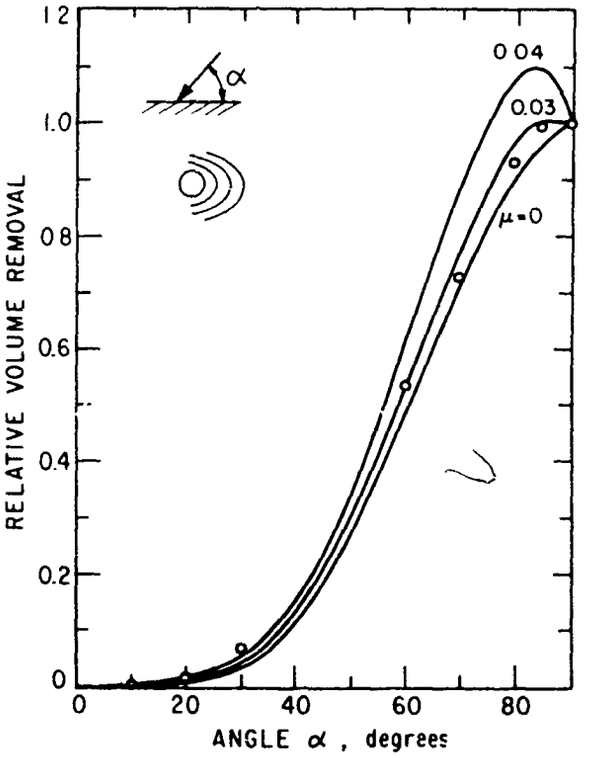

Figure 12. Predicted and Observed Values of the Relative Volume Removal as a Function of Angle for Glass Eroded by 0.0165-Inch-Diameter Steel Shot at 200 ft/sec. Predictions are Made for Three Values of μ, the Coefficient of Friction. The Inserted Sketch Shows the Contact Circle and the Horseshoe Cracks.

force. For impact at high angles (near 90 deg), the spheres should roll rather than slide and the coefficient of friction will be very low. In Figure 12, the predictions are compared with experiment, and it is seen that good agreement is obtained at angles near 90 deg with a coefficient of friction of 0.03.

ANGULAR ABRASIVE PARTICLES IMPACTING AT $\alpha = 90$ DEGREES

In practice, erosion is produced by angular abrasive particles rather than spheres. Since a detailed analysis of this problem, similar to that developed for spheres, does not appear possible at the present time, we present an approximate solution following the approach suggested by Sheldon and Finnie[7] which was later developed by H. L. Oh and Finnie[11].

Surfaces struck by eroding particles typically have the appearance shown in Figure 13. There is relatively little damage under the particle, perhaps because

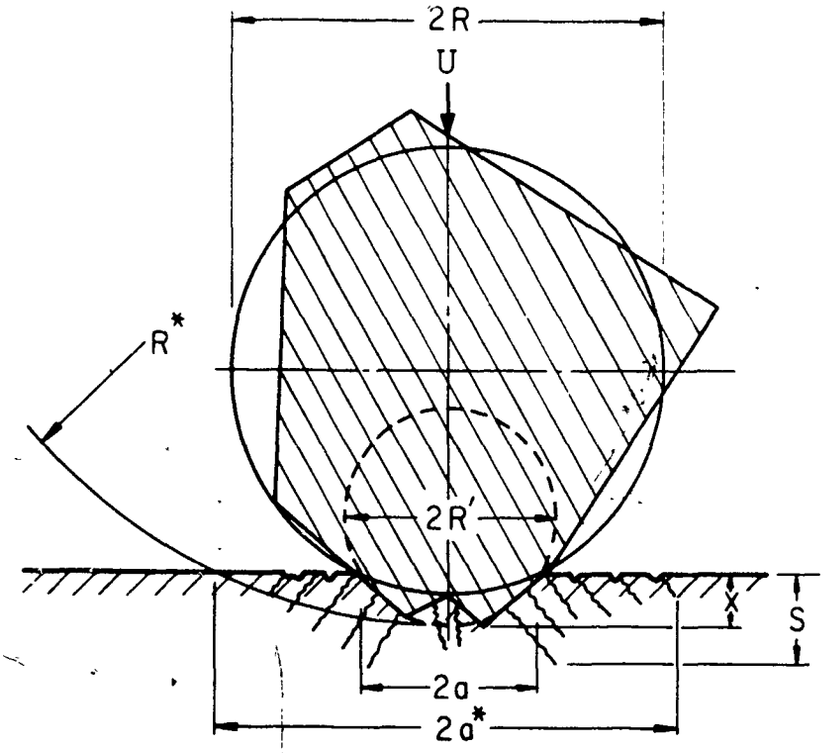

Figure 13. Schematic View of Cracking Due to Particle Impact.

of large hydrostatic compressive stresses at this point. On the surface surrounding the indentation, a fairly extensive region of material is cracked. Based on this observation, we assume that the volume removed by an eroding particle, V_p is proportional to the damaged volume enclosed in the spherical cap of radius R^* and depth S. That is,

$$V_p \propto S^2 R^*$$

In case the particle is not a sphere but is irregular in shape, we may invoke two radii: radius R, which corresponds to a sphere weighing the same as the particle, and radius R', which is effective in producing fracture.

Now, we have to estimate S and R*; as before, we shall take S as proportional to the depth of indentation X obtained from the Hertz solution. We consider R* to be the radius of a much larger indenter than the actual particle, which on the average produces a ring crack at radius a*. This assumption is perhaps not too unreasonable because the cracked material is capable of transmitting load. Since we have seen from Figure 3 that the Hertz equations continue to give a reasonable estimate of load-deflection behavior even after considerable cracking has occurred, we write

$$S \propto \chi \propto R^* \sigma_a^2$$

In order to get a closed solution, we now use the two-parameter Weibull distribution ($\sigma_u = 0$) and from Equation (2) obtain

$$\sigma_{a^*} \chi \propto R^{* - \frac{2}{m+2}}$$

Eliminating σ_{a^*}, we arrive at a relation between R* and χ:

$$R^* \propto \chi^{\frac{m+2}{m-2}}$$

The depth of indentation χ may be estimated readily by assuming that the Hertz solution holds true even after cracking occurs. Then from Timoshenko[3]

$$\chi \propto [R^6/R']^{1/5} U^{4/5}$$

where U is the particle velocity. Finally, volume removed per particle is

$$V_p \propto S^2 R^* \propto \chi^2 R^* \propto \chi^{\frac{3m-2}{m-2}} \left[\frac{R^6}{R'}\right]^{1/5} \left(\frac{3m-2}{m-2}\right) U^{4/5} \left(\frac{3m-2}{m-2}\right)$$

We distinguish two cases:

spherical particle: $R' = R$, $V_p \propto R^{\left(\frac{3m-2}{m-2}\right)} U^{4/5} \left(\frac{3m-2}{m-2}\right)$

irregular particle: $R' =$ constant, $V_p \propto R^{6/5 \left(\frac{3m-2}{m-2}\right)} U^{4/5 \left(\frac{3m-2}{m-2}\right)}$

These expressions for the dependence of volume removal on particle size and velocity have been confirmed. In experiments on six brittle solids over a wide range of velocities and particle sizes,[12] it was indeed found that the volume removal per particle could be written as

$$V_p \propto R^a U^b \qquad \text{for spherical steel shot}$$

$$V_p \propto R^{a'} U^b \qquad \text{for angular silicon carbide particles}$$

A comparison of the predicted and observed values of a, a' and b is given in Figure 14. Except for glass eroded by spherical steel shot, the correlation between theory and experiment is quite good, particularly in view of the number of assumptions involved.

THE BRITTLE-DUCTILE TRANSITION

An interesting consequence of the size-effect on strength of brittle solids is that if the solids are loaded on smaller and smaller regions, the stress required to produce fracture may eventually exceed that required for yield. Thus, we can understand the familiar observation that microhardness or scratch-hardness tests on brittle solids may produce flow rather than fracture.

To estimate the particle size at which ductile behavior should be noticed in erosion testing nominally brittle solids, we need only the parameters of the Weibull distribution and indentation hardness measurements. For glass, this estimate can be made even more directly from the data shown in Figure 4. The mean value of σ_a (the stress at the rim of the contact area) required for fracture is related to the average stress p under the indenter through the Hertz equations as

$$p = \sigma_a \, 2/(1 - 2\nu) \simeq 4\sigma_a \qquad (23)$$

So, for an indenter of radius 10^{-3} inches, we would estimate $\sigma_a \simeq 250{,}000$ psi and $p \simeq 10^6$ psi from Figure 4. Values of the flow pressure $p_{(yield)}$ for glass have been given by Marsh [13] and are typically about 800,000 psi for ordinary hardness tests and about 2,000,000 psi for hardness tests at low temperature where time-dependent effects are absent. The points in Figure 4 are of course for static tests and would be somewhat higher if dynamic loading had been used. So direct comparison is impossible, but it appears that yield should occur before fracture for particles in the range 10^{-4} to 10^{-3} inches. Erosion tests on glass show just such behavior. In Figure 15 it is seen that erosion tests on glass with particles 5×10^{-3} inches and 8×10^{-4} inches in diameter lead to typically brittle behavior, while 3.5×10^{-4}-inch-diameter particles show erosion behavior that is typical of ductile metals. Other aspects of the brittle-ductile transition in erosion have been discussed by Sheldon and Finnie[14].

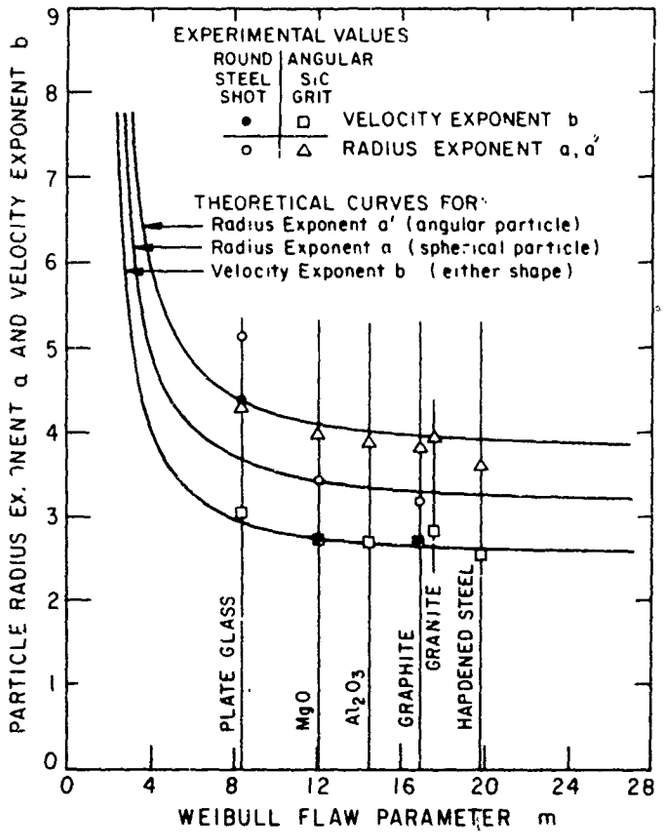

Figure 14. Comparison of Theoretical and Experimental Values of Particle Velocity and Radius Exponents as a Function of the Weibull Flaw Parameter m.

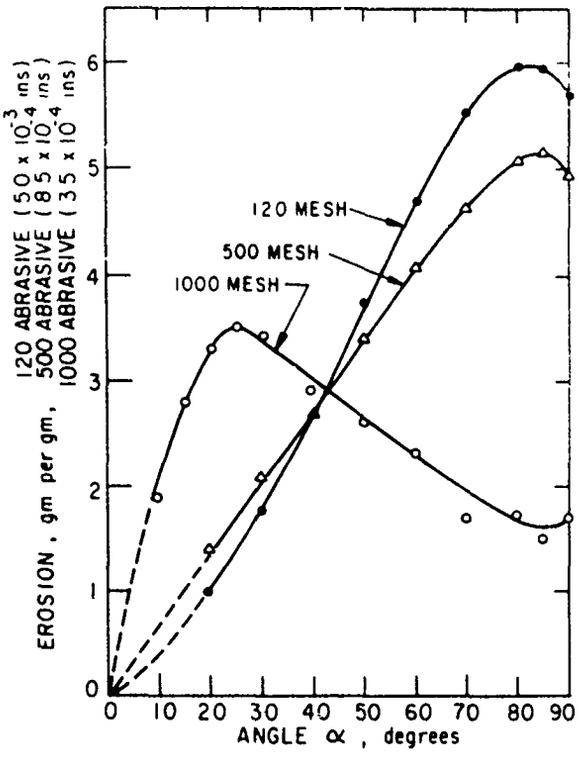

Figure 15. Weight Removal Per Gram of Abrasive as a Function of Particle Approach Angle α for Glass Eroded by Silicon Carbide Particles at 500 ft/sec.

QUANTITATIVE PREDICTION OF VOLUME REMOVAL

In our treatment of erosion due to perpendicular impingement by solid particles, we took the volume removed by a single particle as proportional to the cracked volume produced by a single particle striking a smooth surface. Thus, at least one erosion test must be made on the chosen material before quantitative predictions can be made. We took this approach because the intersection of the fracture patterns from many particles will be a complex process, and more work needs to be done on this topic before a complete quantitative treatment of erosion is possible. However, it may be of value to outline some preliminary considerations in this regard.

Generally, one would expect that the extent of cracking in any brittle solid would depend only on the stress state in the part prior to fracture and on the fracture toughness of the material. This latter quantity could be expressed by an effective surface energy for fracture under plane strain conditions G_{IC} in.-lb/in.^{2} or by the related value of the stress intensity factor K_{IC} lb/in.$^{3/2}$, where

$$G_{IC} = \frac{K_{IC}^2}{E}(1 - \nu^2) \simeq \frac{K_{IC}^2}{E} \tag{24}$$

Normally, the elastic modulus does not appear in elastic solutions for the stresses; but in the present case, because of the change of contact area with load, we would expect the stress state and hence the crack depth in the solid to depend on the modulus as well as on the load (or velocity) and the radius of the indenter.

In our analysis of erosion by spherical particles, we took the depth of cracking as proportional to the depth of indentation. That is,

$$S \sim \frac{p^{2/3}}{R^{1/3}E^{2/3}}$$

where E is a weighted average of the moduli of indenter and surface given by the Hertz equations. A limitation of this expression is that the surface energy for fracture is not included and hence the constant of proportionality must depend on K_{IC} (or G_{IC}).

By contrast, Barenblatt[15], in discussing the literature on fracture under a cylindrical punch, where the contact area does not change with load, showed that

$$S \sim \left(\frac{p}{K_{IC}}\right)^{2/3} \sim \frac{p^{2/3}}{(G_{IC}E)^{1/3}}$$

Very recently, we have made further studies of the depth, S, of the initial ring crack in glass loaded by spherical indenters. Rather than finding S proportional to the indentation χ, i.e., $S \sim p^{2/3}/R^{1/3}$, recent work suggests $S \sim p^{5/6}/R^{1/3}$. Hence from dimensional considerations, we speculate that

$$S \sim \frac{p^{5/6}}{R^{1/3}G_{IC}^{1/3}E^{1/2}} \sim \frac{p^{5/6}}{R^{1/3}K_{IC}^{2/3}E^{1/6}}$$

This new result will not change any of our previous predictions significantly but does suggest that the coefficient of proportionality between the volume $(a^{*2})\chi$ and the volume removed per particle should involve $1/(G_{IC}^{1/3}E^{1/2})$. Representative values of G_{IC} are not easy to obtain for brittle solids. However,

from the literature, we obtained the following approximate values for the materials studied in Figures 7, 8, and 9.

	G_{IC} $\frac{\text{in.-lb}}{\text{in.}}$	E $\frac{\text{lb}}{\text{in.}^2}$	$(G_{IC}^{-1/3} E^{-1/2})$	Observed Ratio of Damage per Particle $+(a^{*2})\chi$
Glass	15×10^{-3}	10×10^{6}	3	9
Graphite	5×10^{-1}	1×10^{6}	3	7
MgO	80×10^{-3}	30×10^{6}	1	1
Al_2O_3	20×10^{-2}	53×10^{6}	0.5	(not tested with shot)

* Relative to MgO as unity

Comparison of the last two columns shows that this method of predicting volume removal is far from precise but may be worth pursuing in future work.

CONCLUSIONS

It has been shown that by considering the region damaged by a single eroding particle we can predict many aspects of the erosion of brittle solids. The effects of impingement angle, particle velocity, particle size and material properties are all included in the analysis. In addition it is possible to predict the transition from brittle to ductile behavior in the case of glass, when the particles are small enough.

At the present state of the analysis, at least one erosion test must be made on the material of interest before erosion rates can be predicted. Further work on the depth of cracking under a single particle and on the interaction of cracks produced by many particles would be desirable. With this information it may be possible to make completely quantitative erosion predictions based on fracture test data.

LITERATURE CITED

1. Finnie, I., EROSION OF SURFACES BY SOLID PARTICLES, Wear, 3, 1970, pp. 87-103.

2. Walker, D. R., and Shaw, M. C., A PHYSICAL EXPLANATION OF THE EMPIRICAL LAWS OF COMMUNICATION, Mining Engineering, 6, 1954, pp. 313-320.

3. Timoshenko, S., THEORY OF ELASTICITY, New York, New York, McGraw Hill Book Company.

4. Weibull, W., A STATISTICAL THEORY OF THE STRENGTH OF MATERIALS, Ingvetenskakad. Handl.,(Stockholm) No. 151, 1939.

5. Oh, H. L., and Finnie, I., THE RING CRACKING OF GLASS BY SPHERICAL INDENTERS, J. Mech. Phys. Solids, 15, 1967, pp. 401-411.

6. Oh, H. L., and Finnie, I., ON THE LOCATION OF FRACTURE IN BRITTLE SOLIDS I-DUE TO STATIC LOADING, to be published in the Int. J. of Fracture Mechanics.

7. Sheldon, G. L., and Finnie, I., THE MECHANISM OF MATERIAL REMOVAL IN THE EROSIVE CUTTING OF BRITTLE MATERIALS, Trans. ASME, 88B, 1966, pp. 393-400.

8. Hamilton, G. M., and Goodman, L. E., THE STRESS FIELD CREATED BY A CIRCULAR SLIDING CONTACT, J. Applied Mechanics, 33, 1966, pp. 371-376.

9. Erdogan, F., and Sih, G. C., ON THE CRACK EXTENSION IN PLATES UNDER PLANE LOADING AND TRANSVERSE SHEAR, Trans. ASME, J. Basic Eng., 1963, pp. 519-527.

10. Oh, K. P. L., ON THE STATISTICAL NATURE OF BRITTLE FRACTURE, Ph.D. Thesis in Mechanical Engineering, University of California, Berkeley, 1970.

11. Oh, H. L., and Finnie, I., AN ANALYSIS OF ROCK DRILLING BY EROSION, Proc. 1st Congress Int. Soc. Rock Mechanics, 2, 1966, pp. 99-104.

12. Sheldon, G. L., EROSION OF BRITTLE MATERIALS, Ph.D. Thesis in Mechanical Engineering, University of California, Berkeley, 1965.

13. Marsh, D. M., PLASTIC FLOW IN GLASS, Proc. Roy. Soc. (London), 279A, 1964, pp. 420-435.

14. Sheldon, G. L., and Finnie, I., ON THE DUCTILE BEHAVIOR OF NOMINALLY BRITTLE MATERIALS IN EROSIVE CUTTING, Trans. ASME, 88B, 1966, pp. 387-392.

15. Barenblatt, G. I., MATHEMATICAL THEORY OF EQUILIBRIUM CRACKS, Advances in Applied Mechanics, (Editors H. L. Dryden and T. von Karman), Vol. 7, Academic Press, 1962, pp. 55-129.

APPENDIX
EROSION TEST EQUIPMENT

For completeness, we include this description of our erosion test apparatus. It is essentially that given by Sheldon[12].

An erosion tester must be capable of accelerating a small but variable mass flow rate of abrasive particles to a predetermined velocity, allow them to impinge on a test specimen, and then be exhausted into a suitable collector. Provision must be made in the tester to vary the angle of attack between the abrasive particle approach direction and the surface of the test specimen. To allow rapid testing of a large number of samples, the tester must be simple and easily operated.

Figure 16 is a schematic view of the apparatus designed to fulfill these objectives. Figure 17 shows photographs of the same equipment. The equipment is designed to be used in two configurations. The first configuration is sed for initial pressure-velocity calibration of the abrasive particles, in which case no erosion sample is in place. In the second configuration the test specimen is eroded with the velocity calibration equipment removed.

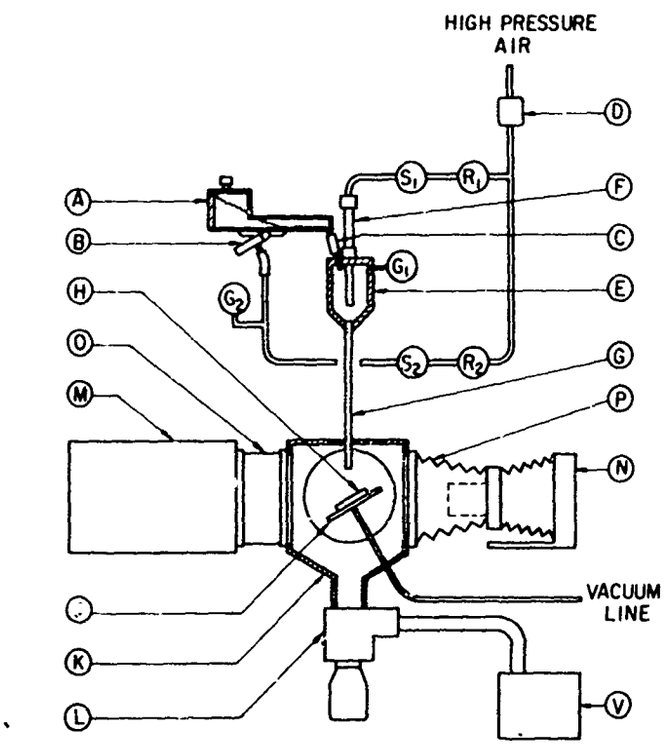

Figure 16. Schematic View of Erosion Test Equipment.

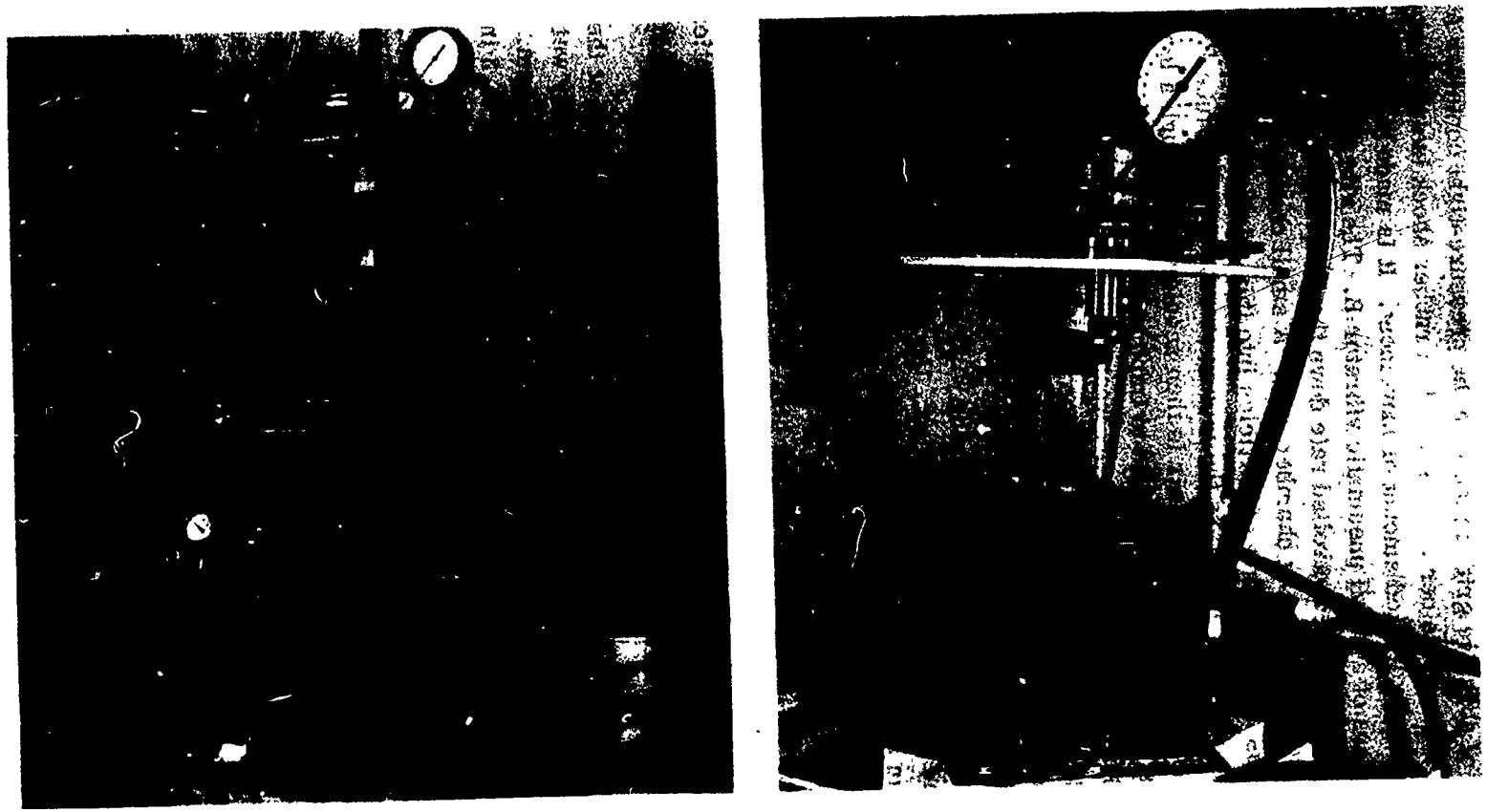

Figure 17. Photographs of Erosion Test Equipment.

In the latter mode, the equipment functions as follows. Referring to Figure 16, a measured amount of abrasive grit is placed in the pressure-tight container A through the screw top. Container A is mounted on rubber shock isolation mounts, and hence is capable of a limited amount of movement. It is made to vibrate at a desired rate by means of a small pneumatic vibrator B. The vibration of the container feeds the particles at a controlled rate down the feed tube and through the flexible connection C into a mixing chamber at E. A small constricting ring in the feed tube insures a uniform flow of particles into this mixing chamber. High-pressure air is filtered at D and enters the mixing chamber through tube F. The abrasive mixed with the high-pressure air is then accelerated through a length of tubing G to the desired velocity and allowed to impinge on the specimen H. The specimen is held firmly to a vacuum plate J, whose angular position α is adjustable from 10 to 90 degrees. The axis of rotation lies on the specimen surface; hence the particle acceleration distance remains constant with changing α. The eroding operation is carried on inside a sealed container K. This container is a box about six inches square and has provision for viewing windows or access doors on all four sides. When erosion tests are carried out, the adjustable vacuum plate J is fitted in place of an access door. This containing box is connected indirectly to a shop type vacuum cleaner V, which has sufficient capacity to maintain a 3- to 4-inch Hg vacuum under all operating conditions. This vacuum system would, probably, not be usable in standard form for high-temperature experiments. After impacting the specimen, the abrasive particles along with all eroded materials are drawn out of the blasting chamber and deposited by a conventional cyclone separator and are picked up in the vacuum cleaner.

A typical test run would proceed as follows. The vacuum plate J is set at the desired impact angle and locked in position. The specimen is accurately weighed and placed on the vacuum plate, being held firmly in position by the vacuum. The specimen is normally 1/8 inch thick by 1 inch wide but may be as long as 3 inches depending on the attack angle α. An accurately weighed amount of abrasive is placed in container A, and the container is sealed. Abrasive charges may range from 0.05 to 100 gm. From previous tests, the air regulators R_1 and R_2 are set with gages G_1 and G_2 to give the desired abrasive velocity and feed rate respectively. Then, with all access doors in position, the vacuum cleaner, the blast air controlled by switch S_1, and the vibrating feeder controlled by switch S_2 are switched on, in that order, and the erosion process begins. The abrasive particles are normally fed at about 10 grams per minute, the abrasive feed rate being readily observed through a window in feeder A. When all the particles have been exhausted, the test is complete. Final weighing of the test specimen then determines the weight of eroded material. If the eroded cavity is found to be deep enough to change the apparent impact angle α significantly, the test is repeated using a reduced abrasive charge.

The vibrating feeder works very well for particles larger than about 500 mesh (0.0008 inch). In tests using particles of 500 mesh or smaller, feeder A is not used. Instead, the high-pressure air inlet tube F is replaced with a similar tube having a small aspirator tube extending into its wall. A small flexible hose is connected to the aspirator tube. The desired charge of abrasive particles is spread in a thin layer in a pan, and the open end of the flexible aspirator hose is passed over the particles to entrain them in the main air blast. The abrasive flow rate is not as uniform using the aspirator as it was using the vibrating feeder; however, the results obtained were very satisfactory. The aspirator was not usable at blast pressure above about 25 psig. This, however, caused no difficulties, as these smaller particles are accelerated to the desired velocities by much lower blast pressures.

In all the erosion tests, the blast tube G was 12 inches long by 0.182 inch inside diameter. The tube material was 304 stainless steel. Because the tube bore wore rather quickly and particle velocity was very sensitive to bore changes, the apparatus was constructed to enable rapid tube changes to be made. In this application, a tube of high hardness ceramic material would have been more suitable.

An important parameter in erosion analysis is the abrasive particle velocity U. This quantity cannot be determined with sufficient accuracy using analytical methods because of the significance of several unknown parameters. For example, it is difficult to account for the effects of impact between the particles and the walls of tube G or between the particles themselves. It was, therefore, decided to determine the particle velocities experimentally.

The technique used for measuring particle velocities was to photograph the particles twice using a double-flash light source M. Knowing the interval between the light flashes and by measuring on the film the distance the particle travels between exposures, the average particle velocities are easily calculated.

The light source used was a commercially available unit, which has a variable flash interval of 5 to 100 microseconds with a flash duration of 0.5 microseconds. A Fresnel lens mounted on the front of the source efficiently accumulated the short-duration light. An opaque tube, 0.6 inch in diameter and 16 inches long formed a light-tight path between the flash unit and the viewing box. The image of the Xenon flash tubes was focused on the camera lens by an adjustment built into the unit.

The camera, shown at N, was a conventional Speed Graphic with 13-inch bellows extension and removable lens board. A 100 mm Zeiss Luminar lens mounted on a 3-inch extension tube provided a capability of 3.5X magnification. The Luminar

lens was especially suitable for this application because of its extreme sharpness and its effective reduction of curvature of field. The lens board of the camera was connected to the view boss by an opaque bellows P, variable in length from 2 to 12 inches. This provided a light-tight path between the view box and the camera, yet allowed the camera to be focused on the abrasive stream at a fixed camera bellows extension or magnification.

Conventional 4 x 5 sheet film was used in the tests. It was found that when film with rating ASA 400 was used, a lens opening of f6.3 provided good exposure. For trial runs, a Polaroid 4 x 5 sheet film adapter was used in the Graphic camera and was found to be very convenient. Polaroid 3000 series film shot at f16 was used and provided good resolution, though not as good as the regular sheet film.

In photographing a stream of abrasive particles, the primary problem was in determining the two positions of the same particle on the doubly exposed film. It was often very easy to confuse two separate particles as being the same particle in its two positions. To reduce the possibility of this mix-up occurring, it was necessary to reduce the number of rebounding particles in the viewing box K. This was effectively accomplished by removing the specimen holder J and allowing the stream of particles to pass straight through the box into the precipitator. In addition, by reducing the feeder pressure, the particle density was reduced so only a few particles were visible in a single exposure.

The procedure used to photograph an abrasive particle was as follows. The camera bellows was set to give the desired magnification, and the camera was carefully focused on the center line of tube G. The double-flash light source was set to give a particle travel distance of about 6 times the particle diameter. The abrasive flow was started and the blast air pressure was set at the desired level. A photograph was then taken by removing the light shield from the film holder and flashing the light source. Because of the precautions taken to eliminate light leakage, no shutter was necessary on the camera.

The particle travel distances were accurately measured using a Zeiss measuring microscope. This instrument permits viewing through the negative at magnifications up to 80X. The built-in measuring system permits an easy measurement to be made between the centers of gravity of the particle images accurate to 1/10,000th of an inch. Abrasive particles as small as 500 mesh (0.0008 inch diameter) could be viewed with this instrument.

In all, about 500 photographs were taken and about 3000 separate measurements were made to obtain calibration curves of particle velocity versus air pressure for different sizes of steel shot and silicon carbide grit.

Unclassified

Security Classification

DOCUMENT CONTROL DATA - R & D

(Security classification of title, body of abstract and indexing annotation must be entered when the overall report is classified)

1. ORIGINATING ACTIVITY *(Corporate author)*
Solar Division of International Harvester Company
San Diego, California

2a. REPORT SECURITY CLASSIFICATION
Unclassified

2b. GROUP

3. REPORT TITLE
STUDY OF THE MECHANISMS OF SAND AND DUST EROSION

4. DESCRIPTIVE NOTES *(Type of report and inclusive dates)*
Final Report

5. AUTHOR(S) *(First name, middle initial, last name)*
Iain Finnie

6. REPORT DATE	7a. TOTAL NO. OF PAGES	7b. NO. OF REFS
December 1970	45	15

8a. CONTRACT OR GRANT NO
DAAJ02-68-C-0056

b. PROJECT NO.
Task 1G162203D14413

c.

d.

9a. ORIGINATOR'S REPORT NUMBER(S)
USAAVLABS Technical Report 70-70

9b. OTHER REPORT NO(S) *(Any other numbers that may be assigned this report)*
Solar Report Number RDR 1625-7

10. DISTRIBUTION STATEMENT
This document is subject to special export controls, and each transmittal to foreign governments or foreign nationals may be made only with prior approval of Eustis Directorate, U.S. Army Air Mobility Research and Development Laboratory, Fort Eustis, Virginia 23604.

11. SUPPLEMENTARY NOTES

12. SPONSORING MILITARY ACTIVITY
Eustis Directorate
U.S. Army Air Mobility R&D Laboratory
Fort Eustis, Virginia

13. ABSTRACT

The fundamental mechanisms by which erosion occurs in brittle solids have been examined.

The erosion process in brittle solids is studied by considering the extent to which a single impacting particle produces fracture in the surface of a brittle solid. By drawing on recent work on the location of fracture in brittle solids, it is possible to predict the effect of such variables as eroding particle size and velocity, angle of impact, material properties, and residual stress. Also, in the case of glass it is possible to predict, approximately, the particle size at which a transition occurs from brittle to ductile behavior.

DD FORM 1 NOV 68 1473 REPLACES DD FORM 1473, 1 JAN 64, WHICH IS OBSOLETE FOR ARMY USE.

Unclassified

Security Classification

14 KEY WORDS	LINK A		LINK B		LINK C	
	ROLE	WT	ROLE	WT	ROLE	WT
Brittle Erosion Mechanism Solid-Particle Erosion Ductile-Brittle Erosion Transition Target Material Properties Engineering Variables Erosive Environments						